ACS OMEGA

http://pubs.acs.org/journal/acsodf

Article

Polyoxygenated Cyclohexenes from *Uvaria grandiflora* with Multi-Enzyme Targeting Properties Relevant in Type 2 Diabetes and Obesity

Mark Tristan J. Quimque, Ryan Joseph Y. Magsipoc, Lloyd Christian J. Llames, Angeli Izza G. Flores, Katherine Yasmin M. Garcia, Andreas Ratzenböck, Hidayat Hussain, and Allan Patrick G. Macabeo*

Cite This: *ACS Omega* 2022, 7, 36856−36864

Read Online

ACCESS | Metrics & More | Article Recommendations | Supporting Information

ABSTRACT: Shikimic acid-derived polyoxygenated cyclohexene natural products commonly occurring in several species of the *Uvaria* represent natural products with promising biological activities. While a number of derivatives have been reported from *Uvaria grandiflora* (*U. grandiflora*), further studies are needed to discover additional bioactive congeners, particularly derivatives with multi-protein target inhibitory properties implicated in diseases such as diabetes and obesity. In this paper, isolation and identification of a new highly oxygenated cyclohexene, uvagrandol (**1**), along with the known compound (-)-zeylenone (**2**) from the DCM sub-extract of *U. grandiflora* following *in vitro* and *in silico* assessment of their enzyme inhibitory properties against α-glucosidase, dipeptidyl peptidase IV, porcine lipase, and human recombinant monoacylglycerol lipase are reported. The structure of **1** was elucidated using 1D and 2D NMR data analysis. The absolute configuration of **1** was established by quantum chemical calculations *via* the Gauge-Independent Atomic Orbital (GIAO) NMR method followed by TDDFT-Electronic Circular Dichroism (ECD) calculations. The structures of the eight possible stereoisomers were optimized by means of DFT calculations (B3LYP/6-31+G[d,p] in vacuum), and then their isotropic shielding tensors were obtained using the GIAO method at mPW1PW91/6-31G(d,p) in chloroform. Through DP4+, the isomer of configuration (1*S*,2*S*,3*R*,6*R*) for **1** was predicted with 96.3% probability. Compounds **1** and **2** significantly inhibited the four target enzymes *in vitro*. Binding studies through molecular docking simulations showed strong binding affinities for (-)-zeylenone (**2**), thus validating the *in vitro* results. Our findings suggest the potential of polyoxygenated cyclohexenes, in particular (-)-zeylenone (**2**), in anti-diabetic and anti-obesity drug discovery.

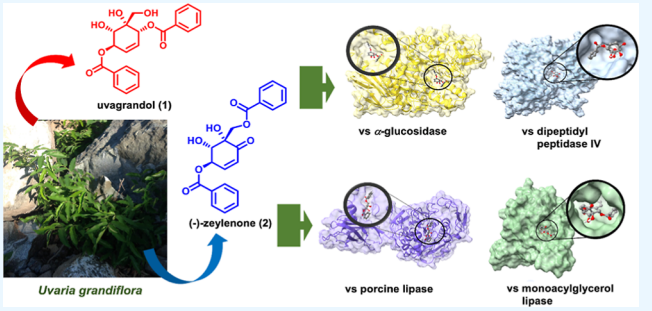

1. INTRODUCTION

The increased incidence of diabetes and obesity has led the World Health Organization to recognize them as epidemics.[1] Based on the WHO data in 2018, 13% of adults aged 18 years suffered from obesity and diabetes in 2016. The alarming rate at which these two metabolic disorders have increased worldwide compounds further with the ongoing COVID-19 pandemic. Around 60−90% of hospitalized patients with COVID-19 have comorbidities, with diabetes and obesity being the most common.[2] In addition, diabetes and obesity can increase the severity of COVID-19 due to the synergy between insulin resistance with hormonal resistance underlying in obesity and diabetes. Thus, it is relevant at the present time to discover new dual-disease-acting compounds with anti-obesity and antidiabetic potentials.[3,4]

The discovery of dual protein-targeting inhibitors is a logical and efficient strategy for developing drugs with multi-disease therapeutic actions. A number of dual- or multi-targeting therapeutics are pursued in the hope of finding a single compound acting on several protein targets. Compounds with multi-targeting properties are advantageous in solving limited efficiencies, poor safety, and resistant profiles of a particular disease target. Advances in bioinformatic platforms and accessibility of structural information of protein targets have allowed the discovery of multi-targeting inhibitors.

For metabolic disorders with multifactorial origins such as diabetes and obesity, plant-derived therapeutics are warranted in order to benefit a good response. Reports on the risk of their adverse effects are limited. There exists also a gap in scientific evidence of plant-derived therapeutic benefits. The Philippines is a highly biodiverse country abounding with plant taxa with medicinal properties. In the Luzon island, the woody shrub

Received: August 28, 2022
Accepted: September 28, 2022
Published: October 7, 2022

Uvaria grandiflora (*U. grandiflora*) Roxb. ex Hornem[5] of the Annonaceae family is found and has been reported to elaborate novel polyoxygenated cyclohexene natural products with antitubercular antibacterial, antioxidant, antiprotozoal, and cytotoxic properties.[6]

As part of our ongoing efforts to explore novel biologically active compounds from Philippine medicinal Annonaceae plants,[7−9] in particular new molecular archetypes exhibiting antidiabetic and anti-obesity properties, secondary metabolites from *U. grandiflora* were investigated, which led to the isolation of a new highly oxidized natural product uvagrandol (**1**) along with (-)-zeylenone (**2**). The enzyme inhibitory activities of **1** and **2** against α-glucosidase, porcine lipase, dipeptidyl peptidase-IV (DPP-IV), and human recombinant monoacylglycerol lipase (MAGL) were also explored *in vitro* and *in silico*.

2. RESULTS AND DISCUSSION

2.1. Plant Material. The air-dried leaves of *U. grandiflora* were extracted three times with DCM/methanol (v/v, 1:1)[6−9] at room temperature. The crude extract was concentrated under reduced pressure to evaporate the organic solvent. The green, syrupy crude extract was fractionated into petroleum ether, DCM, and n-butanol sub-extracts using liquid−liquid extraction with methanolic water (5%) and the DCM sub-extract subjected to silica gel column chromatography. Repeated column chromatography led to the isolation of compounds **1** and **2**. Compound **2** was characterized by matching with its reported ^{1}H and ^{13}C NMR values.[10]

2.2. Structure Characterization of 1 and 2. Compound **1** was isolated as an amorphous pale yellow solid. The molecular formula was deduced as $C_{21}H_{20}O_7$ by HRESIMS, which indicated the presence of 12 double-bond equivalents. The ^{13}C, DEPT-135, and HSQC-DEPT NMR spectra (Figures S2−S4) showed 17 carbon signals for 1 × CH_2, 15 × CH, and 5 × C. The IR spectrum showed the presence of alcohols (3336 cm^{-1}), ester carbonyls (1724 cm^{-1}), and olefinic and aromatic residues (1635 cm^{-1}). The ^{1}H NMR spectrum (Figure S1 and Table 1) contained signals corresponding to AB doublet methylene protons at δ_H 3.68, 4.10 (2H, d, J = 12 Hz, H_2−7), benzoyloxy methines at δ_H 5.83 (dd, J = 7.4, 2.4 Hz, H−3) and δ_H 5.52 (1H, d, J = 3.9 Hz, H−6), oxymethine at δ_H 4.24 (1H, d, J = 7.4 Hz, H−2), two olefinic protons at δ_H 6.04 (1H, dd, J = 2.4, 1.5 Hz, H−4) and δ_H 6.07 (1H, dd, J = 3.9, 1.5 Hz, H−5), and benzoyloxy group protons resonating between δ_H 7.47 and 8.09 (10H).

Table 1. ^{1}H and ^{13}C NMR Spectroscopic Data of 1 ($CDCl_3$)

position	δ_C	δ_H
1	74.0	
2	73.3	4.24 (d, 7.4)
3	74.7	5.83 (dd, 7.4, 2.4)
4	130.3	6.04 (dd, 2.4, 1.5)
5	125.7	6.07 (dd, 3.9, 1.5)
6	71.7	5.52 (d, 3.9)
7	64.8	4.10 (d, 12.0), 3.68 (d,12.0)
1′	129.4	
2′/6′	130.0	8.09 (dd, 8.0, 1.4)
3′/5′	128.6	7.47 (ddd, 8.0, 7.4, 1.4)
4′	133.7	7.60 (dd, 7.4, 1.4)
7′	166.7	
1″	129.2	
2″/6″	129.9	8.03 (dd, 8.0, 1.4)
3″/5″	128.5	7.47 (ddd, 8.0, 7.4, 1.4)
4″	133.6	7.60 (dd, 7.4, 1.4)
7″	166.2	

The presence of these functionalities, coupled with its molecular formula, 12° of unsaturation, and detailed analysis of the ^{1}H NMR and ^{13}C NMR data (Table 1), indicated that compound **1** is a densely hydroxylated cyclohexene with two benzoyl ester groups and planar structure similar to kweichowenol D[10], however with different specific rotations. This is corroborated by homonuclear and heteronuclear correlations derived from the Correlation Spectroscopy (COSY) Heteronuclear Multi-Bond Correlation (HMBC) spectrum (Figures S5 and S6). The relative stereochemistry of the cyclohexene core was established through analysis of the 2D Nuclear Overhauser Effect Spectroscopy (NOESY) NMR spectroscopic data (Figure S7). Correlations between H_2−7 with H−2 and H−6 suggested that H−2, H−6, and H_2−7 are located on the same face of the molecule. A coupling constant of ∼7.3 Hz (^3J) between H−2 and H−3 suggested a trans stereochemistry. Thus, the structure of **1** was elucidated as a new natural product, hitherto assigned the name uvagrandol ((1*R**,4*R**,5*S**,6*S**)-5,6-dihydroxy-5-(hydroxymethyl)-cyclohex-2-ene-1,4-diyl dibenzoate), Figures 1 and 2.

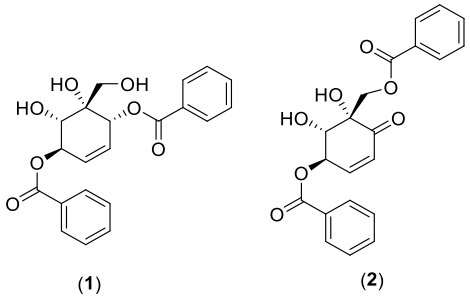

Figure 1. Polyoxygenated cyclohexenes from *U. grandiflora*.

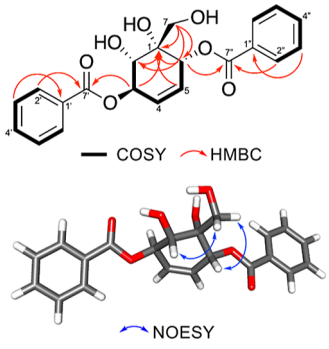

Figure 2. Homonuclear and heteronuclear correlations in **1**.

The structure of uvagrandol (**1**) was confirmed by carrying out quantum chemical calculations through DP4+ NMR probability analysis followed by TDDFT-Electronic Circular Dichroism (ECD) calculations. Since compound **1** has four stereocenters (C−1, C−2, C−3, and C−6), eight possible pairs of enantiomers can be generated, and one from each pair is subjected to DP4+ probability NMR analysis (Figure 3). The proposed structure of **1** based on experimental data is assigned as isomer A, and the rest of the seven stereoisomers were drawn by holding the stereochemistry of C−3 in place. Initially, each of the stereoisomers underwent conformational

https://doi.org/10.1021/acsomega.2c05544
ACS Omega 2022, 7, 36856−36864

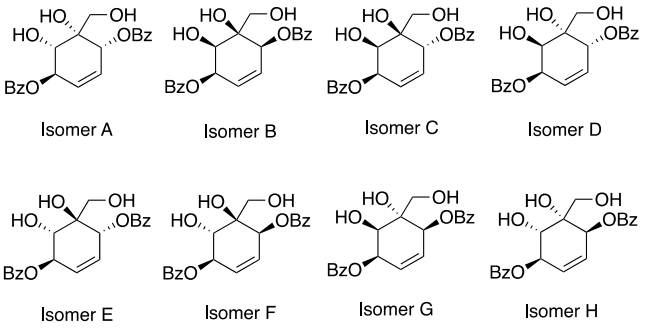

Figure 3. Structures of eight possible stereoisomers for uvagrandol (**1**).

search using Merck molecular force field-94 (MMFF94) to identify low-lying energy conformers. The geometry of the isomers was optimized at the B3LYP/6-31G(d,p) level of theory using a polarizable continuum model (PCM) for chloroform. The isotropic magnetic shielding tensors were computed using the Gauge-Independent Atomic Orbital (GIAO) method at mPW1PW91/6-31G(d,p) (Table S1). The calculated parameters, particularly isotropic shielding and chemical shifts, were compared against experimental ^{1}H and ^{13}C NMR data using the DP4+ method. As shown in Table 2, based on the combined probability of ^{1}H and ^{13}C nuclei, the structure of uvagrandol (**1**) is in agreement with that of isomer A at high probability (94.30%).

Because NMR cannot discriminate between enantiomers, the absolute configuration of uvagrandol (**1**) was further verified by carrying out TDDFT-ECD calculations. Isomer A, with a stereochemical assignment of (1*S*,2*S*,3*R*,6*R*)-**1**, was subjected to theoretical ECD spectra prediction for comparison with experimental spectra. A conformational search was done using MMFF94 to identify stable conformers with equilibrium population >1%. The structures of the stable conformers were re-optimized at the B3LYP/6-31G(d) (PCM/MeCN) level of theory. The conformational search and optimization afforded three conformers which differ in the orientation of the 1-hydroxymethyl moiety, particularly about the rotatable C−1−C−7 bond attaching the methylene bridge to the cyclohexene core.

Conformer **1A**, with an equilibrium population of 93.59%, projected an orientation, which maximizes the hydrogen bonding between hydroxyl groups C−2(OH)/C−7(OH) and vicinal C−1(OH)/C−7(OH) with a $\omega_{C7(OH)\text{-}C7\text{-}C1\text{-}C2}$ torsion angle of −77.05°. The other two stable conformers, **1B** (3.53% population) and **1C** (2.88% population), showed $\omega_{C7(OH)\text{-}C7\text{-}C1\text{-}C2}$ torsion angles of 60.27 and −171.18 °, respectively. TDDFT calculations were performed on all conformers at various levels of theory (PCM/MeCN), particularly at B3LYP/6-31G(d), B97D/TZVP, and ωB97XD/DGDZVP. Of the three levels of theory, the ωB97XD/DGDZVP-calculated ECD spectra, presented as an average based on the Boltzmann distribution of the three conformers, exhibited the best agreement with the experimental ECD spectra (Figures 4 and 5). A 10 nm bathochromic shift was made to correct for underestimation of excitation energies in theoretical calculation. As shown in Figure 4, both spectra displayed two negative Cotton effects (CEs), a sharp peak around λ 200 nm, and a short broader peak at λ 240 nm. The calculated ECD of the enantiomer, on the other hand, showed an opposite spectral pattern.

In the paper of Xu *et al.*, the CD spectroscopic data of kweichowenol D was reported with a structure corresponding to isomer E (Figure 3).[10] To further establish the absolute configuration of uvagrandol (**1**) and distinguish its structure from other reported diastereomers, we determined the theoretical ECD spectrum of isomer E *via* TDDFT calculations and compared it with the reported CD data for kweichowenol D. It was shown that kweichowenol D exhibited a positive CE at λ 235.5 (+3.55) and a negative CE at λ 218.5 (−6.16), which concurs with the TDDFT-ECD spectrum of isomer E with a similar split curve showing a positive CE at 235 nm and a negative CE at around 206 nm (Figure S8). Both theoretical and reported CD spectra have been shown to be similar and displayed a different spectral pattern from compound **1**. Thus, from the results of the DP4+ NMR probability analysis and the TDDFT calculations, we confirm the absolute configuration of uvagrandol (**1**) to be (1*S*,2*S*,3*R*,6*R*).

2.3. *In Vitro* and *In Silico* Biological Activity of 1 and 2. Diabetes is a metabolic disorder characterized by abnormally high plasma glucose levels. Among the strategies to decrease postprandial hyperglycemia is to delay the absorption of glucose by inhibition of carbohydrate hydrolases such as α-glucosidase. α-Glucosidase is the main enzyme involved in the final step of carbohydrate digestion. Hence, α-glucosidase inhibitors can retard the generation of D-glucose from dietary complex carbohydrates and retard glucose absorption. In addition, DPP-IV inhibitors control high blood sugar in adults with type 2 diabetes. Thus, compounds having activities to both enzymes may be promising antidiabetic compounds. Compounds **1** and **2** were screened for their *in vitro* and *in silico* inhibition of α-glucosidase and DPP-IV. As shown in Table 3, both compounds showed high anti-α-glucosidase properties, with (-)-zeylenone (**2**) exhibiting better activity (IC_{50} = 2.62 μM), even higher than the positive control acarbose (IC_{50} = 3.36 μM). To confirm the inhibitory activities of the compounds, uvagrandol (**1**) and (-)-zeylenone (**2**) were docked onto α-glucosidase (PDB ID: 5ZCC) (Figure 6 and Table 3). Compound **1** exhibited a binding score of −8.1 kcal/mol and was bound to the active site through hydrogen bonding with Asp^{327}, Gln^{328}, and Asn^{258}, π-alkyl interactions with Met^{385} and Ala^{200}, and π−π stacking interactions with Phe^{163}. Exhibiting a docking score of −8.6 kcal/mol, **2** was bound through hydrogen bonding with Arg^{411} and Ser^{145} as well as exhibiting π−π stacking interactions with Phe^{146} and Tyr^{388} and π-sulfur interactions with Met^{385} (Figure 6).

Table 2. DP4+ Probabilities of the Eight Possible Isomers of Uvagrandol (1) Calculated at PCM/mPW1PW91/6-31G(d,p)

	percentage probability							
	isomer A (%)	isomer B (%)	isomer C (%)	isomer D (%)	isomer E (%)	isomer F (%)	isomer G (%)	isomer H (%)
DP4+ (^{1}H data)	15.99	4.80	15.66	0.07	26.36	6.21	0.02	30.88
DP4+ (^{13}C data)	97.08	1.15	0.00	0.00	0.00	0.00	0.01	1.76
DP4+ (all data)	96.30	0.34	0.00	0.00	0.00	0.00	0.00	3.36

https://doi.org/10.1021/acsomega.2c05544
ACS Omega 2022, 7, 36856−36864

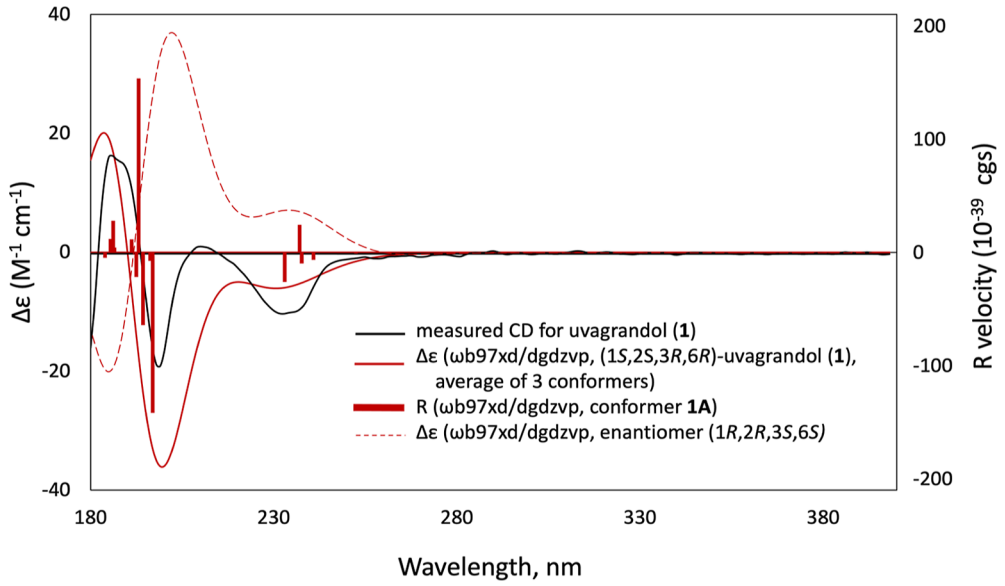

Figure 4. Experimental ECD spectrum of uvagrandol (**1**, black solid curve) compared with ωB97XD/DGDZVP-calculated ECD spectra (red solid curve) for the B3LYP/6-31G(d)-optimized conformers of (1*S*,2*S*,3*R*,6*R*)-**1** and its enantiomer (red dashed curve).

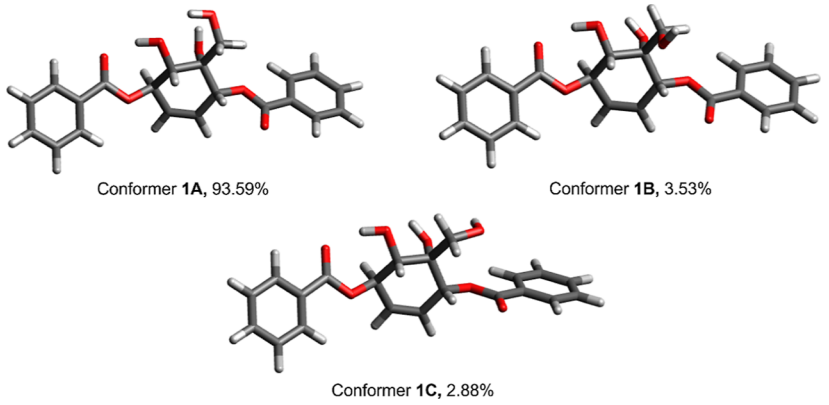

Figure 5. Low-energy conformers (>1%) of (1*S*,2*S*,3*R*,6*R*)-**1** optimized at B3LYP/6-31G(d) (PCM/MeCN).

Table 3. Inhibitory Activity and BE Values of 1 and 2*vs* α-Glucosidase and DPP-IV[a]

test compound	IC_{50}*vs* α-glucosidase (μM)	BE *vs* α-glucosidase (kcal mol^{-1})	IC_{50}*vs* DPP-IV (μM)	BE *vs* DPP-IV (kcal mol^{-1})
1	15.2	−8.0	ND	ND
2	2.62	−8.6	15.7	−8.7
acarbose	3.36	−8.5	ND	ND
sitagliptin	ND	ND	16.9	−8.9

[a]ND: not determined, IC_{50} values are represented as mean based on triplicate measurements.

Because of the promising *in vitro* activity of zeylenone (**2**) against α-glucosidase, the compound was further evaluated for its inhibitory activity against DPP-IV. Based on the assay, compound **2** exhibited potent activity for DPP-IV inhibition (IC_{50} = 15.7 μM), which is comparable to, or even better than, the positive control sitagliptin (IC_{50} = 16.9 μM). As per *in silico* molecular docking analysis, **2** displayed a good topographical fit into the S1 pocket, one of two active pockets of the DPP-IV, with a binding energy (BE) of −8.7 kcal/mol. Both benzoyl substituents participated in T-shaped π−π interactions with Phe^{367}, Tyr^{662}, and Tyr^{666}, while the carbonyl oxygen interacted with Arg^{125} and Asn^{710} through conventional H-bonding.

Inhibition of lipases represents a promising approach to discover the potential of natural products as anti-obesity agents. The mechanism highlights inhibition of triacylglyceride absorption. The success of the only marketed lipase inhibitor orlistat has warranted studies to discover new generation lipase inhibitors with lesser side effects. Thus, the anti-obesity potential of the compounds was likewise assessed *via* inhibitory activities against drug targets for obesity management: pancreatic lipase and MAGL inhibitory activities. As per *in vitro* porcine lipase bioactivity, zeylenone (**2**) demonstrated better activity (IC_{50} = 2.78 μM) as compared to uvagrandol (**1**) and the positive control orlistat (IC_{50} = 5.49 μM). After being docked onto pancreatic lipase, **1** conferred a binding score of −9.5 kcal/mol and demonstrated several interactions, the most notable being hydrogen bonding with Ser^{153}, a known catalytic residue of porcine lipase.[4] Other notable interactions of the complex include π-σ interactions with Val^{260}, π−π stacking interactions with Ty^{115}, and π-alkyl interactions Pro^{181}, Arg^{257}, and Ile^{79}. Exhibiting the highest binding score of −10.3 kcal/mol, **2** demonstrated hydrogen bonding with Phe^{78}, π-σ interactions with Val^{260}, and π−π stacking interactions with

https://doi.org/10.1021/acsomega.2c05544
ACS Omega 2022, 7, 36856−36864

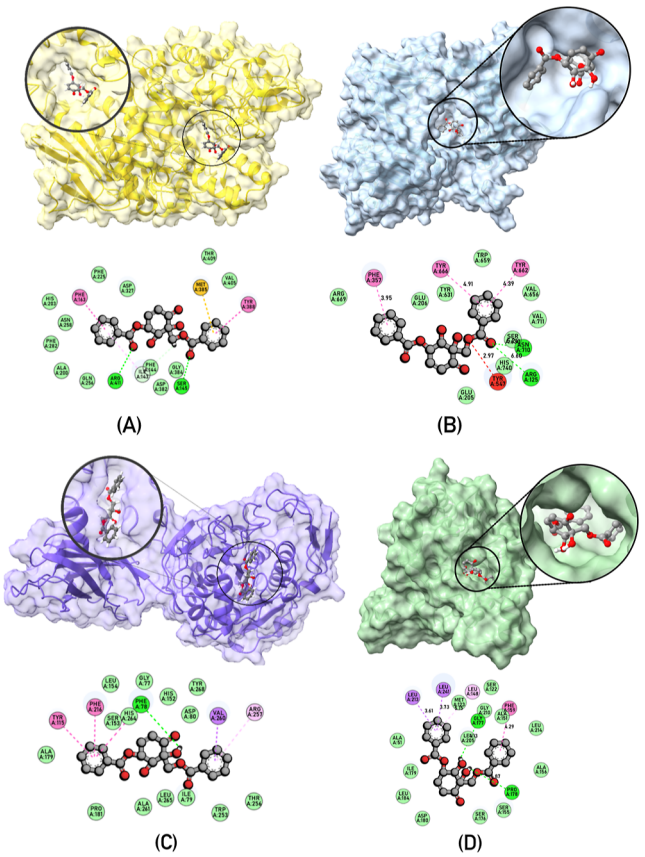

Figure 6. 2D and 3D docking pose of zeylenone (**2**) against (A) α-glucosidase (PDB ID: 5ZCC); (B) DPP-IV (PDB ID: 2RIP); (C) pancreatic lipase (PDB ID: 1ETH); and (D) MAGL (PDB ID: 3PE6).

Ty[115] and Phe[216] (Figure 6). As for the MAGL inhibitory assay, zeylenone (**2**) showed moderate bioactivity with an IC_{50} of 27.90 μM as compared to the positive control (IC_{50} = 10.66 μM). Molecular docking simulation corroborated with these results where JLZ195, the positive control, exhibited better BE (−10.5 kcal/mol) in comparison to that of zeylenone (**2**) (−9.2 kcal/mol) Table 4.

Table 4. Inhibitory Activity and BE Values of 1 and 2*vs* Porcine Lipase and Monoacylglycerol Lipase[a]

test compound	IC_{50}*vs* porcine lipase (μM)	BE *vs* porcine lipase (kcal mol^{-1})	IC_{50}*vs* MAGL (μM)	BE *vs* MAGL (kcal mol^{-1})
1	11.2	−9.5	ND	ND
2	2.78	−10.3	20.90	−9.2
orlistat	5.49	−7.0	ND	ND
JLZ195	ND	ND	10.7	−10.5

[a]ND: not determined, IC_{50} values are represented as mean based on triplicate measurement.

Compounds **1** and **2** were assessed for their adsorption, metabolism, distribution, and excretion (ADME) properties *in silico* to provide a prediction of their potential pharmacokinetic behavior (Table S2). Lipinski's Rule of Five (LRo5) considers the parameters of lipophilicity, number of H-bond donors, number of H-bond acceptors, and molecular weight,[11] while Veber's rules consider the number of rotatable bonds and the topological polar surface area (TPSA), a measure of the extent that polar atoms contribute to the outer surface of the molecule.[12] Both LRo5 and the Veber rules use physicochemical parameters to estimate the oral bioavailability of drug candidates. As per LRo5 and Veber rules, compounds **1** and **2** had zero violations. Both **1** and **2** were identified by SwissADME as non-inhibitors of five major isoforms (CYP1A2, CYP2C19, CYP2C9, CYP2D6, and CYP3A4) of human cytochrome P_{450} (Table S3). The synthetic accessibility (SA) scores of **1** and **2** were 4.49 and 4.32, respectively. The SA score ranges from 1 (easy to synthesize) to 10 (difficult to synthesize). Therefore, both compounds are neither complex nor challenging to synthesize for large-scale production. In addition, SwissADME provides a graphical representation to predict passive gastrointestinal absorption and blood−brain barrier (BBB) permeation through the BOILED-Egg (Brain Or IntestinaL EstimateD permeation method) plot, which plots the lipophilicity of a compound against its TPSA.[13] Compounds located in the yellow region (yolk) of the BOILED-Egg plot are highly likely to be BBB permeants, whereas compounds located in the white region of the plot are non-BBB permeants.[10] Both compounds **1** and **2** are positioned within the white region. Therefore, **1** and **2** were predicted to exhibit properties characteristic of small molecules exhibiting a high probability of gastrointestinal tract absorption (Figure 7).

3. CONCLUSIONS

In summary, two polyoxygenated cyclohexene derivatives **1** and **2** were isolated and identified from the DCM sub-extract of *U. grandiflora*. Uvagrandol (**1**) is a new oxidized cyclohexene derivative from *U. grandiflora*. Its structure was elucidated using comprehensive spectroscopic and computational methods. (-)-Zeylenone (**2**) exhibited strong inhibitory activity against α-glucosidase, pancreatic lipase, and DPP-IV *in vitro* and *in silico*, demonstrating its potential in discovering new antidiabetic and anti-obesity drug chemotypes.

4. MATERIALS AND METHODS

4.1. General Experimental Procedures. Optical rotations were obtained using a Jasco P-2000 polarimeter at 589 nm using a 1 mL quartz cell (10 cm path length) for solutions in MeOH. IR data were recorded using a Shimadzu Prestige-21 FTIR spectrophotometer (ATR). NMR spectra were recorded at ambient probe temperature using a Bruker Avance 400 MHz Kryo spectrometer. All NMR spectra were acquired in $CDCl_3$ and referenced to solvent signals at δ_H 7.26 and δ_C 77.16. HRESIMS data were acquired using an Agilent Q-TOF 6540 UHD mass spectrometer (sodium formate). Preparative HPLC purification was performed at room temperature with an Agilent 1100 series preparative HPLC system; binary pump system; column: Kromasil RP C18, particle size 7 μm, dimensions 250 × 25 mm; mobile phase: MeOH or ACN and water; flow rate 20 mL/min; diode-array UV detector; and 226 fraction collector. Thin-layer chromatography was performed using Merck silica gel 60 F_{254} pre-coated plates (0.25 mm) and visualized by UV fluorescence quenching and staining with vanillin−H_2SO_4. Column chromatography was performed on Merck 60 silica gel (0.063−0.200 mm) or Merck 60 flash silica gel (0.040−0.063 mm) stationary phases.

4.2. Plant Material. The leaves of *U. grandiflora* were collected in the lowland forests of Rizal, Santa, Ilocos Sur, Philippines (17°32′ N, 120°27′ E), in January 2013. Voucher

https://doi.org/10.1021/acsomega.2c05544
ACS Omega 2022, 7, 36856−36864

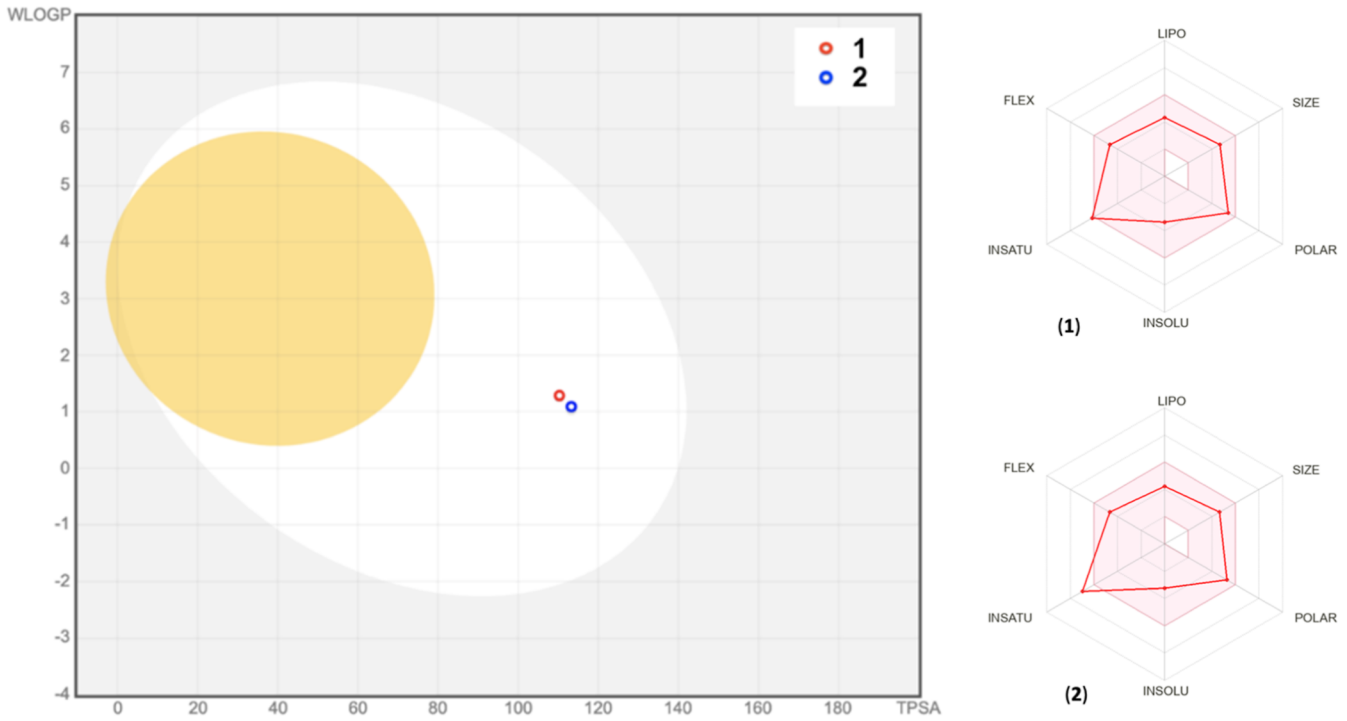

Figure 7. BOILED-egg plot and bioavailability radar plots for gastrointestinal tract absorption and brain permeation prediction of compounds **1** and **2**.

specimens (USTH11028) were deposited at the University of Santo Tomas Herbarium, Manila, Philippines.

4.3. Extraction. The air-dried leaves were ground (4.5 kg s) and subjected to cold percolation with DCM-MeOH (1:1),[6−9] and the resulting crude extracts were concentrated under reduced pressure (45 °C) to give 285.0 g of green, syrupy crude extract. The crude extract was suspended in water and extracted sequentially with petroleum ether, DCM, and n-butanol and concentrated *in vacuo* (45 °C) to obtain the DCM sub-extract.

4.4. Isolation of 1 and 2. The DCM sub-extract was fractionated using silica gel vacuum liquid chromatography. Gradient elution was carried out using EtOAc in petroleum ether (10%) followed by gradients of MeOH in EtOAc (10%) to give eight fractions. Fraction one (3.9 g) was chromatographed on silica gel using 3:1 petroleum ether-EtOAc to give compound **2** (48.6 mgs). Sub-fraction six was further purified using RP-18 HPLC with gradients of acetonitrile in water to afford compound **1** (3.3 mg).

(-)−Uvagrandol (**1**). Amorphous pale yellow solid; $[\alpha]_D^{25}$ −51° (MeOH). IR (DRS) ν_{max} 3336 (br), 1724, 1635, 1454, 1145, 1107, 1091, 617 cm^{-1}; HR-ESI-MS *m/z* 385.1210 $[M + H]^+$ (calcd for $C_{21}H_{21}O_7$, 385.1209).

4.5. Biological Activity Assays. *4.5.1. α-Glucosidase Inhibitory Assay.* The enzymatic assay was performed by the hydrolysis of a chromogenic substrate *p*-nitrophenyl-α-glucopyranoside (*p*-NPG) using a previously described procedure[14] with slight modifications. Compounds **1** and **2** were dissolved in DMSO to obtain a 1 mg/mL stock solution. From the stock solution, six different concentrations of 0.1, 1, 5, 10, 100, and 250 μg/mL were prepared using 100 mM phosphate buffer (pH = 6.8). The α-glucosidase inhibitory assay was carried out by initially incubating the mixture in a clear microwell plate containing 8 μL of the test compound, 112 μL of phosphate buffer, and 20 μL of α-glucosidase solution (0.2 U/mL) at 37 °C for 15 min. Initial absorbance was measured at 405 nm using a Promega Glomax Multi Detection Plate Reader. Subsequently, a volume of 20 μL of substrate (2.5 mM *p*-NPG) was added. The reaction mixture was further incubated at 37 °C for another 15 min, and the reaction was terminated by the addition of 80 μL of 0.2 M Na_2CO_3 solution. The final absorbance of the reaction mixture was measured at 405 nm. Acarbose, the positive control, was prepared in the same manner, and a sample blank was prepared for each sample replacing the enzyme with phosphate buffer. All assays were performed in triplicate. The enzymatic hydrolysis of *p*-nitrophenyl glucopyranoside to *p*-nitrophenol was assessed through the change in the absorption at 405 nm using the following formula

$$\text{glucosidase inhibition (\%)} = \left[\left(1 - \frac{\Delta ABS_{\text{test compound}}}{\Delta ABS_{\text{control test}} - \Delta ABS_{\text{control blank}}}\right) \times 100\right]$$

The glucosidase inhibitory activities of compounds **1** and **2** were plotted against the logarithmic concentrations, and the IC_{50} values were determined.

4.5.2. DPP-IV Inhibitory Assay. DPP-IV activity was assessed using a DPP-IV inhibitor screening assay kit (Cayman Chemical, Ann Arbor, MI, USA), which provided a fluorescence-based method for screening DPP-IV inhibitors. The assay used the fluorogenic substrate, Gly-Pro-amino-methylcoumarine (AMC), to measure DPP-IV activity. Cleavage of the peptide bond by DPP released the free AMC group, resulting in fluorescence that could be analyzed using an excitation wavelength of 350−360 nm and an emission wavelength of 450−465 nm.

The tested compounds were initially dissolved in DMSO to produce a 50 mM stock solution and subsequently diluted to

https://doi.org/10.1021/acsomega.2c05544
ACS Omega 2022, 7, 36856−36864

the required concentrations using DMSO, and then they were added to a 96-well plate in a final volume of 10 μL and a final concentration of 50 μM. The assay procedure is described briefly according to the manufacturer's protocols as follows: diluted assay buffer (30 μL) and diluted enzyme solution (10 μL) were added to a 96-well plate containing 10 μL of solvent (blank) or solvent-dissolved test compounds. The reaction was initiated by adding 50 μL of a diluted substrate solution, and the plate was incubated for 30 min at 37 °C. After incubation, fluorescence with an excitation wavelength of 350 nm and an emission wavelength of 450 nm was monitored using a plate reader (Promega GloMaxExplorer, Germany). IC_{50} values were derived from experimental data using the sigmoidal dose−response fitting of GraphPad Prism software. Final values were obtained from three replicate experiments.

4.5.3. Pancreatic Lipase Assay. The lipase inhibitory activities of compounds **1** and **2** were investigated using a colorimetric assay that quantifies the release of *p*-nitrophenol butyrate (*p*-NPB) according to previous reports[15,16] with some modifications. A stock solution of 1 mg/mL test compounds dissolved in DMSO was used from which four different working solutions with the concentrations of 0.1, 1.0, 5.0, and 10 μg/mL were prepared. The porcine pancreatic lipase enzyme (Sigma-Aldrich, USA) solution was freshly prepared by dissolving 1 mg of porcine pancreatic lipase in 1 mL of tris-HCl buffer (2.5 mmol Tris, pH = 7.4, and 2.5 mmol NaCl). Lipase assay was performed in triplicate measurements by pre-incubating the mixture containing 20 μL of each test compound, 10 μL of pancreatic lipase enzyme, and 70 μL of Tris-HCl buffer in a 96-well microwell plate at 25 °C for 15 min. The enzymatic hydrolysis was initiated upon the addition of 15 μL of *p*-NPB, which was then incubated at 37 °C for 30 min. The amount of *p*-nitrophenolate ions generated by the reaction was monitored by measuring the absorbance at 405 nm using a Promega Glomax Multi Detection Plate Reader. Orlistat and DMSO were used as positive and negative controls, respectively. The lipase inhibitory activity was evaluated with and without an inhibitor by using the following formula

$$\text{lipase inhibition (\%)} = \left[100 - \left(\frac{B-b}{A-a} \times 100\right)\right]$$

where A is the activity of the test compounds without an inhibitor, a is the negative control without an inhibitor, B is the activity of the test compounds with an inhibitor, and b is the negative control with an inhibitor. IC_{50} values of compounds **1** and **2** were calculated using the least-squares regression line of the plots of the logarithm of the sample concentration (log) versus the pancreatic lipase inhibitory activity (%).

4.5.4. Human Recombinant MAGL Inhibition Assay. Activity against human recombinant MAGL was assessed using an MAGL inhibitor screening assay kit (Cayman Chemical, Ann Arbor, MI, USA), which provided an absorbance-based method for screening MAGL inhibitors. For 100% initial activity wells, 150 μL of 1X Assay Buffer, 10 μL of MAGL enzyme, and 10 μL of DMSO were added to three wells; for background Wells, 160 μL of 1X Assay Buffer and 10 μL of DMSO to three wells were added; and for inhibitor/positive control wells, 150 μL of 1X Assay Buffer, 10 μL of MAGL enzyme, and 10 μL of inhibitor or positive control JZL 195 inhibitor were added to the inhibitor wells. Contents of the wells were mixed by pipetting gently up and down and incubated for 15 min at room temperature. Reactions were initiated by adding 10 μL of the MAGL substrate to all the wells being used. The 96-well plate was shaken for 10 s to mix and incubated for 10 min at room temperature. Absorbance was read at 405−415 nm using a plate reader (Promega GloMaxExplorer, Germany). IC_{50} values were derived from experimental data using the sigmoidal dose−response fitting of GraphPad Prism software. Final values were obtained from three replicate experiments.

4.6. Computational Calculations. *4.6.1. Quantum Mechanical Calculations.* All quantum mechanical calculations were carried out using Gaussian 16W, while the visualization of results was done on GaussView 6.0.[17,18] All conformational analyses were performed using the Avogadro (version 1.1.1) platform,[19] which included a search for low-lying energy conformations using the MMFF94 molecular mechanics and conformer optimization following the steepest descent algorithm. The geometries of all stable conformations underwent re-optimization *via* DFT calculations with the B3LYP/6-31G(d) basis set on a PCM with chloroform as the solvent model. The calculated energies, taken as the sum of electronic and zero-point energies, were used to estimate the Boltzmann population for each conformer. For DP4+ NMR analysis, the isotropic magnetic shielding tensors were estimated using the GIAO method at mPW1PW91/6-31G-(d,p) (PCM/MeCN) for ^{1}H and ^{13}C nuclei. Unscaled chemical shifts (δ^{u}) were calculated using tetramethylsilane (TMS) as the reference standard according to the following expression $\delta^{u} = \sigma_0 - \sigma^{x}$, where σ^{x} is the Boltzmann-averaged shielding tensor (over all significantly populated conformations) and σ_0 is the shielding tensor of the reference TMS computed at the said level of theory. σ^{x} was calculated as the Boltzmann averaging according to the following equation

$$\sigma^{x} = \frac{\sum_i \sigma_i^{x} e^{(-E_i/RT)}}{\sum_i e^{(-E_i/RT)}}$$

where σ is the shielding constant for nucleus x in conformer i, R is the molar gas constant, T is the temperature set at 298 K during calculations, and E is the energy of conformer i obtained during geometry optimization and NMR calculation. The scaled (sDP4+), unscaled (uDP4+), and DP4+ probabilities were estimated from experimental and calculated parameters (chemical shifts and isotropic shielding values) as per the developed mathematical tool by Grimblat *et al.*[20]

For the TDDFT-ECD calculations, all stable conformers of isomer A, with equilibrium calculation >1%, underwent re-optimization *via* DFT calculations with the B3LYP/6-31G(d) basis set at PCM/MeCN. The calculated energies, taken as the sum of electronic and zero-point energies, were used to estimate the Boltzmann population for each conformer. The optimized geometries were then subjected to TDDFT using the following levels of theory/basis sets: B3LYP/6-31G(d), B97D/TZVP, and wB97XD/DGDZVP (PCM/MeCN). A Gaussian distribution function was used to generate the ECD curve from the calculated rotatory strength values with a 3000 cm^{-1} half-height width.[21,22]

4.6.2. Molecular Docking Studies. Compounds **1** and **2** were subjected to molecular docking simulations with the enzymes pancreatic lipase (PDB ID: 1ETH), α-glucosidase (PDB ID: 5ZCC), DPP-IV (PDB ID: 2RIP), and MAGL (PDB ID: 3PE6) to assess their binding characteristics. The enzymes were fetched from the protein data bank as co-

https://doi.org/10.1021/acsomega.2c05544
ACS Omega 2022, 7, 36856−36864

crystallized structures. USCF Chimera (version 1.13.1) was used to facilitate the removal of bound residues and minimization of structures. Dock-prepping of ligand and protein structures was done using Antechamber, and molecular docking was performed using the BFGS algorithm of AutoDock Vina (version 1.1.2).[23] Validation of the docking protocol was done *via* the redocking experiment of the co-crystallized ligands. The conformational protein−ligand structure was visualized and analyzed using Biovia Discovery Studios (version 4.1).[24]

4.6.3. Drug-Likeness, ADME, and Toxicity Prediction. The computational prediction of the pharmacokinetic (ADME) properties of **1** was done using the SwissADME program (Molecular Modeling Group, Swiss Institute of Bioinformatics 2019, online version).[12,25] The ORISIS Property explorer program (Thomas Sander, Idorsia Pharmaceuticals Ltd.,[26] 2017) was employed for *in silico* toxicity prediction.

■ ASSOCIATED CONTENT

Supporting Information

The Supporting Information is available free of charge at https://pubs.acs.org/doi/10.1021/acsomega.2c05544.

1D and 2D NMR, HR-ESIMS spectroscopic data for compound **1**; experimental and theoretical ECD spectrum of **1** and its enantiomer; GIAO isotropic magnetic shielding constants of the isomers of **1**; and ADME profiles of **1** and **2** (PDF)

■ AUTHOR INFORMATION

Corresponding Author

Allan Patrick G. Macabeo − *Laboratory for Organic Reactivity, Discovery and Synthesis (LORDS), Research Center for the Natural and Applied Sciences, University of Santo Tomas, Manila 1015, Philippines;* orcid.org/0000-0001-7972-106X; Email: agmacabeo@ust.edu.ph, allanpatrick_m@yahoo.com

Authors

Mark Tristan J. Quimque − *Laboratory for Organic Reactivity, Discovery and Synthesis (LORDS), Research Center for the Natural and Applied Sciences, University of Santo Tomas, Manila 1015, Philippines; The Graduate School, University of Santo Tomas, Manila 1015, Philippines; Department of Chemistry, College of Science and Mathematics, Mindanao State University-Iligan Institute of Technology, Iligan City 9200, Philippines;* orcid.org/0000-0003-0269-5590

Ryan Joseph Y. Magsipoc − *Laboratory for Organic Reactivity, Discovery and Synthesis (LORDS), Research Center for the Natural and Applied Sciences, University of Santo Tomas, Manila 1015, Philippines*

Lloyd Christian J. Llames − *Laboratory for Organic Reactivity, Discovery and Synthesis (LORDS), Research Center for the Natural and Applied Sciences, University of Santo Tomas, Manila 1015, Philippines*

Angeli Izza G. Flores − *Laboratory for Organic Reactivity, Discovery and Synthesis (LORDS), Research Center for the Natural and Applied Sciences, University of Santo Tomas, Manila 1015, Philippines*

Katherine Yasmin M. Garcia − *Laboratory for Organic Reactivity, Discovery and Synthesis (LORDS), Research Center for the Natural and Applied Sciences, University of Santo Tomas, Manila 1015, Philippines*

Andreas Ratzenböck − *Institut für Organische Chemie, Universität Regensburg, Regensburg D-93053, Germany*

Hidayat Hussain − *Leibniz-Institut für Pflanzenbiochemie, Halle D-06120, Germany*

Complete contact information is available at: https://pubs.acs.org/10.1021/acsomega.2c05544

Author Contributions

A.P.G.M. carried out the conceptualization, investigation, supervision, formal analysis, writing, editing, and reviewing. M.T.J.Q. performed the investigation, formal analysis, writing, and editing. R.J.Y.M. completed the investigation, formal analysis, and writing. L.C.J.L. executed the investigation, formal analysis, and writing. A.I.G.F. conducted the conceptualization, investigation, and formal analysis. K.Y.M.G. worked on the investigation, formal analysis, writing, and editing. A.R. did the investigation and formal analysis. H.H. participated in the investigation, formal analysis, and writing.

Notes

The authors declare no competing financial interest.

■ ACKNOWLEDGMENTS

This work was supported in part by the International Foundation for Science (grant no. F/5376-1).

■ REFERENCES

(1) Chobot, A.; Górowska-Kowolik, K.; Sokołowska, M.; Jarosz-Chobot, P. Obesity and diabetes-Not only a simple link between two epidemics. *Diabetes/Metab. Res. Rev.* **2018**, *34*, No. e3042.

(2) Stefan, N.; Birkenfeld, A. L.; Schulze, M. B. Global pandemics interconnected—Obesity, impaired metabolic health and COVID-19. *Nat. Rev. Endocrinol.* **2021**, *17*, 135−149.

(3) Santos, A.; Magro, D. O.; Evangelista-Poderoso, R.; Saad, M. J. A. Diabetes, obesity, and insulin resistance in COVID-19: Molecular interrelationship and therapeutic implications. *Diabetol. Metab. Syndrome* **2021**, *13*, 23.

(4) Macabeo, A. P. G.; Pilapil, L. A. E.; Garcia, K. Y. M.; Quimque, M. T. J.; Phukhamsakda, C.; Cruz, A. J. C.; Hyde, K. D.; Stadler, M. Alpha-glucosidase and lipase-inhibitory phenalenones from a new species of Pseudolophiostoma originating from Thailand. *Molecules* **2020**, *25*, 965.

(5) Notarte, K. I. R.; Devanadera, M. K. P.; Mayor, A. B. R.; Cada, M. C. A.; Pecundo, M. H.; Macabeo, A. P. G. Toxicity, antibacterial, and antioxidant activities of fungal endophytes Colletotrichum and Nigrospora spp. isolated from Uvaria grandiflora. *Philipp. J. Sci.* **2019**, *148*, 503−510.

(6) Macabeo, A. P. G.; Flores, A. I. G.; Fernandez, R. A. T.; Budde, S.; Faderl, C.; Dahse, H.-M.; Franzblau, S. G. Antitubercular and cytotoxic polyoxygenated cyclohexane derivatives from Uvaria grandiflora. *Nat. Prod. Res.* **2021**, *35*, 5229−5232.

(7) Macabeo, A. P. G.; Letada, A. G.; Budde, S.; Faderl, C.; Dahse, H.-M.; Franzblau, S. G.; Alejandro, G. J. D.; Pierens, G. K.; Garson, M. J. Antitubercular and cytotoxic chlorinated seco-cyclohexenes from Uvaria alba. *J. Nat. Prod.* **2017**, *80*, 3319−3323.

(8) Macabeo, A. P. G.; Martinez, F. P. A.; Kurtán, T.; Tóth, L.; Mándi, A.; Schmidt, S.; Heilmann, J.; Alejandro, G. J. D.; Knorn, M.; Dahse, H.-M.; Franzblau, S. G. Tetrahydroxanthene-1,3(2H)-dione derivatives from Uvaria valderramensis. *J. Nat. Prod.* **2014**, *77*, 2711−2715.

(9) Quimque, M. T.; Notarte, K. I.; Letada, A.; Fernandez, R. A.; Pilapil, D. Y.; Pueblos, K. R.; Agbay, K. R.; Dahse, J. C.; Wenzel-Storjohann, H.-M.; Tasdemir, A.; Khan, D.; Wei, A.; Gose Macabeo, D.-Q.; Macabeo, A. P. G. Potential cancer- and Alzheimer's disease-

targeting phosphodiesterase inhibitors from Uvaria alba: Insights from in vitro and consensus virtual screening. *ACS Omega* **2021**, *6*, 8403−8417.
(10) Liao, Y.-H.; Xu, L.-Z.; Yang, S.-L.; Dai, J.; Zhen, Y.-S.; Zhu, M.; Sun, N.-J. Three cyclohexene oxide from Uvaria grandiflora. *Phytochemistry* **1997**, *45*, 729−732.
(11) Xu, Q. M.; Liu, Y. L.; Zou, Z. M.; Yang, S. L.; Xu, L. Z. Two new polyoxygenated cyclohexenes from Uvaria kweichowensis. *J. Asian Nat. Prod. Res.* **2009**, *11*, 24−28.
(12) Lipinski, C. A.; Lombardo, F.; Dominy, B. W.; Feeney, P. J. Experimental and computational approaches to estimate solubility and permeability in drug discovery and development settings. *Adv. Drug Deliv. Rev.* **2012**, *64*, 4−17.
(13) Veber, D. F.; Johnson, S. R.; Cheng, H.-Y.; Smith, B. R.; Ward, K. W.; Kopple, K. D. Molecular properties that influence the oral bioavailability of drug candidates. *J. Med. Chem.* **2002**, *45*, 2615−2623.
(14) Daina, A.; Zoete, V. A BOILED-Egg to predict gastrointestinal absorption and brain penetration of small molecules. *ChemMedChem* **2016**, *11*, 1117−1121.
(15) Li, Y.; Li, C.; Xu, Q.; Kang, W. Antioxidant, α-glucosidase inhibitory activities in vitro and alloxan-induced diabetic rats' protective effect of Indigofera stachyodes Lindl. root. *J. Med. Plant Res.* **2012**, *6*, 1524−1531.
(16) Bustanji, Y.; Issa, A.; Mohammad, M.; Mohammad, H.; Tawah, K.; Alkhatib, H.; Almasri, I.; Al-Khalidi, B. Inhibition of hormone sensitive lipase and pancreatic lipase by Rosmarinus officinalis extract and selected phenolic constituents. *J. Med. Plant Res.* **2010**, *4*, 2235−2242.
(17) Jaradat, N.; Zaid, A.; Hussein, F.; Zaqzouq, M.; Aljammal, H.; Ayesh, O. Anti-lipase potential of the organic and aqueous extracts of ten traditional edible and medicinal plants in Palestine: A comparison study with Orlistat. *Medicines* **2017**, *4*, 89.
(18) Frisch, M. J.; Trucks, G. W.; Schlegel, H. B.; Scuseria, G. E.; Robb, M. A.; Cheeseman, J. R.; Scalmani, G.; Barone, V. M.; Petersson, G. A.; Nakatsuji, H.; Caricato, M.; Li, X.; Hratchian, H. P.; Izmaylov, A. F.; Bloino, J.; Zheng, G.; Sonnenberg, J. L.; Hada, M.; Ehara, M.; Toyota, K.; Fukuda, R.; Hasegawa, J.; Ishida, M.; Nakajima, T.; Honda, Y.; Kitao, O.; Nakai, H.; Vreven, T.; Montgomery, J. A., Jr.; Peralta, J. E.; Ogliaro, F.; Bearpark, M. J.; Heyd, J.; Brothers, E. N.; Kudin, K. N.; Staroverov, V. N.; Kobayashi, R.; Normand, J.; Raghavachari, K.; Rendell, A. P.; Burant, J. C.; Iyengar, S. S.; Tomasi, J.; Cossi, M.; Rega, N.; Millam, N. J.; Klene, M.; Knox, J. E.; Cross, J. B.; Bakken, V.; Adamo, C.; Jaramillo, J.; Gomperts, R.; Stratmann, R. E.; Yazyev, O.; Austin, A. J.; Cammi, R.; Pomelli, C.; Ochterski, J. W.; Martin, R. L.; Morokuma, K.; Zakrzewski, V. G.; Voth, G. A.; Salvador, P.; Dannenberg, J. J.; Dapprich, S.; Daniels, A. D.; Farkas, O.; Foresman, J. B.; Ortiz, J. V.; Cioslowski, J.; Fox, D. J.*Gaussian 16 (Revision A.03)*: Wallingford, CT, 2016.
(19) Garcia, K. Y. M.; Phukhamsakda, C.; Quimque, M. T. J.; Hyde, K. D.; Stadler, M.; Macabeo, A. P. G. Catechol-bearing polyketide derivatives from. Sparticola junci. *J. Nat. Prod.* **2021**, *84*, 2053−2058.
(20) Hanwell, M. D.; Curtis, D. E.; Lonie, D. C.; Vandermeersch, T.; Zurek, E.; Hutchison, G. R. An advanced semantic chemical editor, visualization, and analysis platform. *J. Cheminf.* **2012**, *4*, 17−34.
(21) Grimblat, N.; Zanardi, M. M.; Sarotti, A. M. Beyond DP4: An improved probability for the stereochemical assignment of isomeric compounds using quantum chemical calculations of NMR shifts. *J. Org. Chem.* **2015**, *80*, 12526−12534.
(22) Garcia, K. Y. M.; Quimque, M. T. J.; Primahana, G.; Ratzenböck, A.; Cano, M. J. B.; Llaguno, J. F. A.; Dahse, H.; Phukhamsakda, C.; Surup, F.; Stadler, M.; et al. COX inhibitory and cytotoxic naphthoketal-bearing polyketides from Sparticola junci. *Int. J. Mol. Sci.* **2021**, *22*, 12379.
(23) Garcia, K. Y. M.; Quimque, M. T. J.; Lambert, C.; Schmidt, K.; Primahana, G.; Stradal, T. E. B.; Ratzenböck, A.; Dahse, H.; Phukhamsakda, C.; Stadler, M.; et al. Antiproliferative and cytotoxic cytochalasins from Sparticola triseptata inhibit actin polymerization and aggregation. *J. Fungi* **2022**, *8*, 560.
(24) Wang, J.; Wang, W.; Kollman, P. A.; Case, D. A. Automatic atom type and bond type perception in molecular mechanical calculations. *J. Mol. Graph. Model.* **2006**, *25*, 247−260.
(25) Trott, O.; Olson, A. J. Software news and update AutoDock Vina: Improving the speed and accuracy of docking with a new scoring function, efficient optimization, and multithreading. *J. Comput. Chem.* **2010**, *31*, 455−461.
(26) Daina, A.; Michielin, O.; Zoete, V. SwissADME: A free web tool to evaluate pharmacokinetics, drug-likeness and medicinal chemistry friendliness of small molecules. *Sci. Rep.* **2017**, *7*, 42717.

https://doi.org/10.1021/acsomega.2c05544
ACS Omega 2022, 7, 36856−36864